Multi-dimensional Eigenwave Multiplexing (MEM): A General Modulation for LTV Channels

Zhibin Zou and Aveek Dutta

Department of Electrical and Computer Engineering
University at Albany SUNY, Albany, NY 12222 USA
{zzou2, adutta}@albany.edu

Abstract—**OFDM and OTFS modulations have demonstrated their efficacy in mitigating interference in time and frequency domains respectively, caused by path delays and Doppler shift. However, no modulation technique exists to address Inter-Doppler Interference (IDI) resulting from time-varying Doppler. Additionally, both OFDM and OTFS require supplementary precoding to mitigate Inter-User Interference (IUI) in MU-MIMO channels. To address these limitations, we present a general modulation for any multi-dimensional channel, based on Higher Order Mercer's Theorem (HOGMT) [1], which has been shown to decompose multi-dimensional channels into independent subchannels. The proposed method, called Multi-dimensional Eigenwave Multiplexing (MEM) modulation, employs jointly orthogonal *Eigenwaves*, decomposed from the multi-dimensional channel as subcarriers, thereby simultaneously canceling interference from all the Degrees of Freedom (DoF). We show that MEM modulation achieves diversity gain in the eigen domain, which in turn achieves total diversity across each DoF *e.g.*, space (users/antennas), time-frequency and Doppler-delay. The accuracy and generality of MEM modulation are validated through simulation in three types of channels, achieving up to *two orders of magnitude* improvement in BER over OTFS.**

Keywords—**Eigen decomposition, multi-dimensional channel, Interference cancellation, Multiplexing, OTFS.**

I. INTRODUCTION

Inter-Symbol Interference (ISI) due to multipath delays is mitigated in OFDM by transmitting symbols in frequency domain [2]. On the other hand, Doppler effect causes Inter-Carrier Interference (ICI), which is addressed by transmitting symbols in the Doppler-delay domain, as in OTFS modulation [3]. However, in rapidly time-varying channels, *both the multipath delays and the Doppler vary over time and frequency*, leading to interference in the Doppler-delay domain, which is commonly referred to as IDI [4]. Receivers have been investigated to mitigate IDI for OTFS symbols [4], [5]. However, these additional steps cannot ensure interference-free communication in the Doppler-delay domain, especially for rapidly time-varying channels. Figure 1 shows the progression of various modulation schemes to mitigate ISI, ICI and IDI due to path difference (Δx), velocity difference ($\Delta x'$) and acceleration difference ($\Delta x''$). Each method is designed to achieve orthogonal subcarriers in the time, time-frequency and Doppler-delay domains respectively. However, these cannot provide subcarriers in other dimensions ($\Delta y^{(m)}$) that do not have simple Fourier bases such as space domain in MU-MIMO, requiring additional precoding to cancel spatial
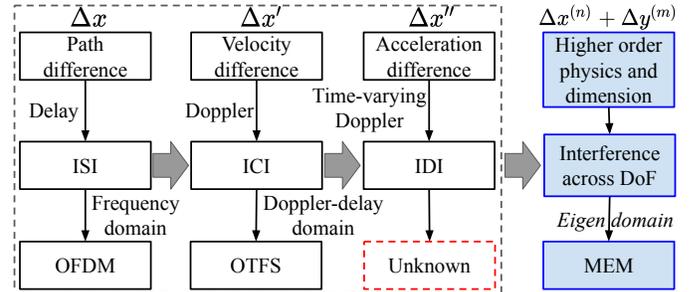
Figure 1: *OFDM and OTFS cancel ISI and ICI respectively but cannot remove interference due to higher order physics, which results in IDI. These are also incapable of canceling interference in the spatial dimension. MEM is a general modulation technique to cancel inference across all the DoF by defining subcarriers in eigen domain, called Eigenwaves.*

interference [6]. Therefore, we postulate designing jointly orthogonal subcarriers in the domains represented by high order physics and/or dimensions is desirable, as it is relatively less variant and cause minimum interference across DoF.

Recently, HOGMT has been proposed as a mathematical tool to decompose multi-dimensional channels, as represented by its *kernel*, which yields independent subchannels along each DoF [1], [7]. We leverage this to develop *Multi-dimensional Eigenwave Multiplexing (MEM)* modulation which employ the jointly orthogonal *Eigenwaves* decomposed from the high-dimensional channel as subcarriers. Symbols on these subcarriers achieve orthogonality across each DoF, thereby simultaneously cancel interference from all dimensions. It is also important that the optimal subcarriers are strictly Eigenwaves in order to remain orthogonal during transmission over the channel. It is well known that complex exponentials, used as OFDM subcarriers are common eigenfunctions for Linear Time-Invariant (LTI) channels. However, there are no such predefined eigenfunctions for general Linear Time-Varying (LTV) channel. We provide a refresher on channel kernel decomposition using HOGMT in Section III-C to contextualize the contributions of this work and clarity.

OTFS uses subcarriers obtained by Symplectic Fourier Transform (SFT), while MEM obtains its subcarriers by HOGMT. These subcarriers are orthogonal in the Doppler-delay domain, while that of MEM are orthogonal in the eigen domain. Further, OTFS requires CSI at the receiver side
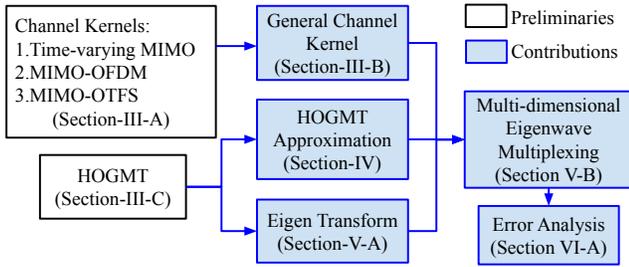
Figure 2: Paper outline: contributions and novelty

only, while `MEM` requires CSI at both the transmitter and receiver side. Although this can be viewed as a potential cost to implement `MEM`, it is quite common to require CSI at the transmitter in modern wireless systems [8]. Also, OTFS cannot directly generalize to higher dimensional channels. For instance, it requires additional precoding for MIMO channels as it cannot achieve spatial orthogonality in the Doppler-delay domain. In theory, OTFS is a special case of `MEM` as it achieves orthogonal Eigenwaves for rapidly time-varying channels as well as in higher dimensions, eliminating the need for additional processing and precoding to simultaneously cancel IDI and IUI. Figure 2, shows the connection between the preliminary concepts required for `MEM` and the contributions of this work, which are summarized as follows[1]:

- We formulate the asymmetric channel kernel for time-varying MIMO, MIMO-OFDM and MIMO-OTFS channels and generalize it for any multi-dimensional channel.
- We prove that approximation by finite eigenfunctions obtained by HOGMT for multi-dimensional asymmetric kernel is optimal in MMSE sense.
- We define *Eigenwave Transform*, which transfers all the DoF to a unified eigen domain. This is applied to design the Multi-dimensional Eigenwave Multiplexing (`MEM`) modulation and show that the Eigenwaves are optimal subcarriers for joint orthogonality across all the DoF.
- We formulate an error metric, *Soft Orthogonality* to evaluate the robustness of `MEM` and show its generality for varying channels. Then we provide a trade-off between the BER and throughput.
- We evaluate `MEM` under three different channels. Two of these are rapidly time-varying channels with different time-evolution intervals and the third is a MU-MIMO channel to show that `MEM` does not require any additional precoding. Finally, we present the PAPR and show the BER and throughput under imperfect CSI.

II. Related work

Rapidly Time-Varying Wireless Channels: There are many instances in modern wireless networks where the receivers may move at very high speeds, causing the geometry of the physical channel to change rapidly, causing rapidly time-varying channels [10], [11]. In this case, the time-frequency and Doppler-delay domains are correlated and hence induce

[1]This manuscript is a extension of the prior work [9].

Table I: Performance gap in rapidly time-varying channels

Applications	Sources of variation	Performance Gap
V2X, HST, UAV	Time-varying scatterers, UAV attitude, high Doppler	**BER at 20 dB:** $\approx 10^{-2}$ [12], [13]
MIMO, XL/MU-MIMO	Time-varying multipath, spatial visibility regions	**Target Metrics:** $10^{-6} <$ **BER** $< 10^{-4}$
mmWave, RIS, VLC, THz	Time-varying blockage and reflection angles, air absorption	

a time-varying Doppler causing interference in the Doppler-delay domain. Table I highlights the challenges of communicating in rapidly time-varying channels, which can stem from various features of the channel, such as time-varying Doppler in Vehicle-to-Everything (V2X), High-Speed Train (HST) and Unmanned Aerial Vehicle (UAV) channels; time-varying multipath in MU-MIMO channels; and time-varying blockage and reflection angles in Reconfigurable Intelligent Surfaces (RIS), Terahertz (THz) links, and Visible Light Communications (VLC). Unfortunately, the State-of-The-Art (SoTA) methods only achieve modest error rates that require **2-4 orders of magnitude** improvement.

Communications in Multi-dimensional Channels: The input-output relations and analysis of MIMO-OTFS systems can be found in [14], [15]. Channel estimation for MIMO-OTFS is investigated in [16], [17], [18], [19], which provide the CSI for equalization and precoding [20], [6], [21]. However, these techniques treat the interference in the space domain and Doppler-delay domain independently, failing to achieve joint orthogonality. A jointly spatio-temporal precoding for multi-dimensional channels is presented in [1]. However, it utilizes eigenfunctions to construct the whole signal instead of transmitting symbols over independent subchannels, making it energy inefficient and sensitive to CSI errors.

Eigen Approximation Problem: Karhunen–Loève Theorem (KLT) approximation is proven to be optimal for the random process approximation by finite eigenfunctions in [22] and Eckart–Young–Mirsky Theorem shows that SVD is optimal for low-rank matrix approximation [23]. Nyström approximation [24] shows rank-k approximation using SVD is optimal for Symmetric Positive Semi-Definite (SPSD) matrix. However, there is no optimality analysis for eigenfunction approximation for asymmetric multi-dimensional kernels. For the implementing eigen approximation, [25] presents a black-box approach for SVD decomposition, which is applicable for matrices. [26] proposed a method for extracting eigenfunctions based on Mercer's Theorem. However, it does not show the optimality of the approximation and is only applicable for symmetric kernels.

III. Channel Kernel and Decomposition

In order to design a general modulation, a unified expression for LTV channels is necessary. Therefore, we begin by deducing the kernels for *three* known multi-dimensional channels from elementary principles [27], followed by a general formulation for *multi-dimensional channel kernel*. The kernels are summarized in Table II for comparative understanding.

A. Kernels of (Common) Multi-dimensional Channels

1) *Case 1: Time-varying MIMO (4-D) Channel*

In LTV channels, the transmitted signal $s(t)$ is impacted by the underlying physics of the channel, described by path delays and Doppler shift to produce the received signal $r(t)$ [11] as,

$$r(t) = \sum_{p=1}^{P} h_p s(t - \tau_p) e^{j2\pi\nu_p t} \tag{1}$$

where h_p, τ_p and ν_p are the path attenuation factor, time delay and Doppler shift for path p, respectively. We omit the noise term for simplicity. Then (1) is expressed in terms of the overall delay τ and Doppler shift ν as

$$r(t) = \iint S_H(\nu, \tau) s(t-\tau) e^{j2\pi\nu t} \, d\tau \, d\nu \tag{2}$$

$$= \int h(t, \tau) s(t-\tau) \, d\tau \tag{3}$$

where $S_H(\nu, \tau)$ is the (Doppler-delay) spreading function, which describes the combined attenuation factor for all paths in the Doppler-delay domain. The time-varying impulse response $h(t, \tau)$ is related to $S_H(\nu, \tau)$ as,

$$h(t, \tau) = \int S_H(\nu, \tau) e^{j2\pi t\nu} \, d\nu \tag{4}$$

Extending $h(t, \tau)$ to MIMO case, $H_{u,u'}(t, \tau)$ denotes the time-varying impulse response between the u'-th transmit antenna and the u-th received antenna. Therefore, the multi-user (or multi-antenna) version of $h(t, \tau)$ [28] is a tensor,

$$\mathbf{H}(t, \tau) = \begin{bmatrix} H_{1,1}(t, \tau) & \cdots & H_{1,u'}(t, \tau) \\ \vdots & \ddots & \vdots \\ H_{u,1}(t, \tau) & \cdots & H_{u,u'}(t, \tau) \end{bmatrix} \tag{5}$$

and the received signal in (3) is extended as,

$$r_u(t) = \int \sum_{u'} H_{u,u'}(t, \tau) s_{u'}(t - \tau) d\tau$$

$$= \int \sum_{u'} K_{u,u'}(t, t') s_{u'}(t') dt' \tag{6}$$

where $K_{u,u'}(t, t') = H_{u,u'}(t, t-t')$ is the 4-D MIMO channel kernel following the definition of kernel in [29], [11]. Then, (6) can be rewritten using the kernel as[2],

$$r(u, t) = \iint K_H(u, t; u', t') s(u', t') \, du' \, dt' \tag{7}$$

In general, the channel tensor, $\mathbf{H}(t, \tau)$ is asymmetric, i.e., $\exists i, j$ pair, such that $H_{i,j}(t, \tau) \neq H_{j,i}(t, \tau)$. Therefore, by definition, channel kernel, $K_H(u, t; u', t')$ is also asymmetric.

2) *Case 2: MIMO-OFDM (4-D) Channel*

Proposition 1. *The continuous form of OFDM input-output relation for LTV, in the frequency domain is given by,*

$$r(f) = \int b(f, \nu) s(f - \nu) d\nu \tag{8}$$

[2]Note that (7) represents the 2-D convolution integral over space and time DoF at the Tx and Rx, where $t' = t - \tau$ and u' are the variables at the Tx.
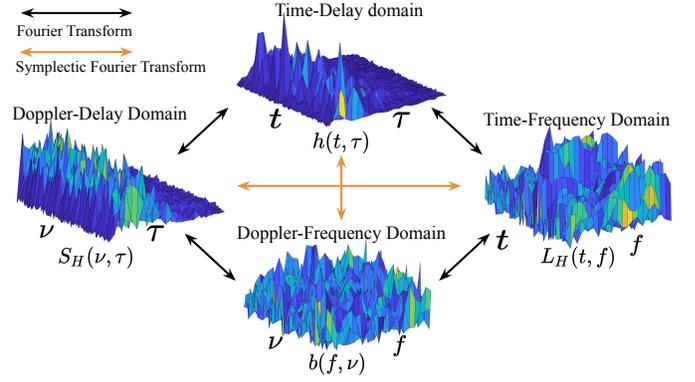
Figure 3: Representation domains of LTV channel: OTFS design 2-D orthogonal subcarriers in the Doppler-delay domain and transfer $S_H(\nu, \tau)$ to $L_H(t, f)$ by SFT and combine the frequency dimension by IFFT to form the time domain symbols. While for LTI channels, $h(t, \tau)$ and $S_H(\nu, \tau)$ collapse to $h(\tau)$; $b(f, \nu)$ and $L_H(t, f)$ collapses to $H(f)$. OFDM combines carriers in the frequency domain to time symbols by IFFT.

where $b(f, \nu)$[3] is the (frequency domain) transfer function [29]. Further, the continuous form of the input-output relation using the MIMO-OFDM kernel, $K_B(u, f; u', f')$ is given by,

$$r(u, f) = \iint K_B(u, f; u', f') s(u', f') \, du' \, df' \tag{9}$$

Proof. For notational compactness, rewrite (3) in matrix form, $\mathbf{r} = \mathbf{h}\mathbf{s}$, where $\mathbf{h}$ is the time-domain channel matrix. Then the frequency domain input-output relation is given by multiplying both sides by the M-point DFT matrix, $\mathbf{F}_M$ on both sides.

$$\underbrace{\mathbf{F}_M \mathbf{r}}_{\check{\mathbf{r}}} = \mathbf{F}_M \mathbf{h}\check{\mathbf{s}} = \underbrace{\mathbf{F}_M \mathbf{h}\mathbf{F}_M^H}_{\mathbf{b}} \underbrace{\mathbf{F}_M \mathbf{s}}_{\check{\mathbf{s}}} \implies \check{\mathbf{r}} = \mathbf{b}\check{\mathbf{s}} \tag{10}$$

Note that $\mathbf{F}_M \mathbf{h} \mathbf{F}_M^H$ is the SFT of $\mathbf{h}$ as shown in Figure 3 and in [30]. Then the continuous form of $\mathbf{b}$ is given by,

$$b(f, \nu) = \iint h(t, \tau) e^{j2\pi(t\nu - f\tau)} \, dt \, d\tau \tag{11}$$

Meanwhile, both $\check{\mathbf{r}}$ and $\check{\mathbf{s}}$ represent the signals in the frequency domain. Therefore, using (11) we can derive the OFDM input-output relation for LTV channels as,

$$r(f) = \int b(f, \nu) s(f - \nu) d\nu \tag{12}$$

Furthermore, extending $b(f, \nu)$ to the MIMO case as $B(f, \nu)$,

$$r_u(f) = \int \sum_{u'} B_{u,u'}(f, \nu) s_{u'}(f - \nu) d\nu \tag{13}$$

Similarly, the kernel input-output relation is given as

$$r(u, f) = \iint K_B(u, f; u', f') s(u', f') \, du' \, df' \tag{14}$$

This follows in the same spirit as defining (7) using (6). □

[3](8) is an archaic form of frequency domain input-output relation for LTV channels in [29], which defines $b(f, \nu)$ as *"Input Spectrum Output Spectrum relation"*. Since this formulation predates OFDM, we believe that it is necessary to prove (8) for MIMO-OFDM in LTV channels using contemporary formulations for OFDM in the literature based on DFT/IDFT.

Table II: Multi-dimensional asymmetric channel kernels in wireless communication

Channel type	Signal domain	Interference type	Input-output relation of channel kernel
Time-varying MIMO [1], [28]	Space-time domain	IAI-ISI	$r(u,t) = \iint K_H(u,t;u',t')s(u',t')du'dt'$
MIMO-OFDM [31], [32]	Space-frequency domain	IAI-ICI	$r(u,t) = \iint K_B(u,f;u',f')s(u',f')du'df'$
MIMO-OTFS [30], [33]	Space-Doppler-delay domain	IAI-IDI	$r(u,\tau,\nu) = \iint K_{DD}(u,\tau,\nu;u',\tau',\nu')s(u',\tau',\nu')du'd\tau'd\nu'$
General multi-dimensional channel	All the DoF	All the DoF	$r(Z) = \int K(Z;Z')s(Z')\,dZ'$

3) *Case 3: MIMO-OTFS (6-D) Channel*

In the literature, OTFS is often written using the Zak representation [30], [33] of (1) as,

$$\mathcal{Z}_r(\tau,\nu) = \sum_{p=1}^{P} h_p e^{j2\pi v_p(\tau-\tau_p)} \mathcal{Z}_s(\tau-\tau_p, \nu-\nu_p) \quad (15)$$

where $\mathcal{Z}_r(\tau,\nu)$ is the Zak transform of $r(t)$ given by,

$$\mathcal{Z}_r(\tau,\nu) \triangleq \sqrt{T}\sum_k r(\tau+kT)e^{-j2\pi k\nu T} \quad (16)$$

where T is the symbol duration. Denote $r(\tau,\nu) = \mathcal{Z}_r(\tau,\nu)$ and $s(\tau,\nu) = \mathcal{Z}_s(\tau,\nu)$ and rewrite (15) as,

$$r(\tau,\nu) = \iint h_{dd}(\tau,\nu;\tau',\nu')s(\tau-\tau',\nu-\nu')\,d\tau'\,d\nu' \quad (17)$$

where $h_{dd}(\tau,\nu;\tau',\nu')d\tau'd\nu'$ describes the combined path gains for all paths in the delay and Doppler-shift range $(\tau',\tau'+d\tau')$ and $(\nu',\nu'+d\nu')$ respectively.

Following similar extensions for MIMO as in previous cases and defining the kernel, (17) is written using the MIMO-OTFS kernel in the space-Doppler-delay domain as,

$$r(u,\tau,\nu) = \iint K_{DD}(u,\tau,\nu;u',\tau',\nu')s(u',\tau',\nu')du'd\tau'd\nu' \quad (18)$$

Remark 1. *The received OTFS symbol at an antenna (u) is the integral of the channel kernel, K_{DD} multiplying all the OTFS symbols over the space-Doppler-delay domain that is responsible for IAI and IDI. Ideally, if the Doppler shift and delay are integer multiples of the time and frequency grids, then the kernel is 0 at other symbols, meaning there is no IDI [33]. However, this ideal OTFS waveform is difficult to achieve in practice because: (a) The perfect division of time-frequency grids may not be practical in channels with high order physics; 2) For multi-path Doppler-delay channels, as the delay and Doppler shifts are different on each path, there is no common factor satisfying the integer multiple requirements. Therefore, in general, OTFS waveform is unable to avoid IDI [30]. Hence we formulate this kernel for further analysis.*

B. Generalized Kernel of Multi-dimensional Channels

Based on the kernel formulations above, the input-output relation of *any* wireless channel (without considering noise) can be modeled as a mapping of the signal at the transmitter to the signal at the receiver by a channel kernel, K as,

$$r(z_1,\ldots,z_k) = \int \ldots \int K(z_1,\ldots,z_k;z_1',\ldots,z_k')s(z_1',\ldots,z_k')dz_1'\ldots dz_k' \quad (19)$$

where $(z_1,\ldots,z_k)$ and $(z_1',\ldots,z_k')$ are the degrees of freedom (*e.g.*, space, time, frequency, delay, Doppler, etc.) at the receiver and the transmitter, respectively. In general, for communication systems $P=Q$. For brevity, henceforth we denote $Z=(z_1,\ldots,z_k)$ and $Z'=(z_1',\ldots,z_k')$, rewriting (19) as,

$$r(Z) = \int K(Z;Z')s(Z')\,dZ' \quad (20)$$

In general, (20) is applicable to any higher-dimensional kernel that may incorporate joint interference between any number of DoFs that are unique to a particular communication paradigm such as scattering angle, polarization, etc. [34], [35].

Remark 2. *At the transmitter, the signal, $s(Z)$ is transmitted in Z domain (also the transmitter DoF), which is converted to the signal in Z' domain, $s(Z')$ during convolution. The convolution (during propagation over LTV), projects $s(Z')$ onto the channel kernel K, which transfers the signal to the Z domain (DoF at the receiver) as $r(Z)$ with the interference across Z' domain (DoF). Common multi-dimensional channel kernels are special cases of this, given by (7), (14) and (18).*

C. Kernel Decomposition

A generalized version of Mercer's Theorem, called High Order Generalized Mercer's Theorem (HOGMT) has been recently proposed in [1]. This presents a mathematically principled approach to decompose multi-dimensional asymmetric channel kernels like in (20), into low-dimension, jointly orthogonal eigenfunctions, which is expressed as,

$$K(Z;Z') = \sum_{n=1}^{\infty} \sigma_n \psi_n(Z)\phi_n(Z') \quad (21)$$

where $\mathbb{E}\{\sigma_n\sigma_n'\}=\lambda_n\delta_{nn'}$. λ_n is the n-th eigenvalue and $\psi_n(Z)$ and $\phi_n(Z')$ are orthonormal eigenfunctions, i,e.,

$$\int \phi_n(Z')\phi_{n'}^*(Z')dZ'=\delta_{nn'} \text{ and } \int \psi_n(Z)\psi_{n'}^*(Z)dZ=\delta_{nn'} \quad (22)$$

These eigenfunctions are referred as *dual eigenfunctions* that exhibit the important *duality* property,

$$\int K(Z;Z')\phi_n^*(Z')\,dZ' = \sigma_n\psi_n(Z) \quad (23)$$

IV. CHANNEL KERNEL APPROXIMATION

Duality property is critical for using the eigenfunctions as independent subchannels in practice. (23) suggests that when one of the eigenfunctions is transmitted through a multi-dimensional channel kernel, it is transferred to its dual eigenfunction, scaled only to the corresponding eigenvalue (or subchannel gain). Therefore, the orthonormality and duality

of the eigenfunction, unambiguously allow us to transmit symbols over independent subchannels in the eigen domain by employing dual eigenfunctions as subcarriers. Note that in this context, *each subchannel/subcarrier is a pair of dual eigenfunctions, $\phi_n(Z')$ and $\psi_n(Z)$.*

HOGMT provides us a mathematical tool to decompose any kernel into an infinite number of eigenfunctions. However, in reality, we can only utilize a finite number of eigenfunctions to approximate the kernel. To achieve maximum energy efficiency, it is desirable to use the least number of eigen components to approximate (most part of) the kernel. Therefore, the general approximation problem is formulated as minimizing the number of eigenfunctions, N that limits the kernel approximation error below some threshold,

$$\underset{\hat{K}}{\arg\min} \quad N \quad \text{s.t} \quad \|K(Z;Z') - \hat{K}(Z;Z')\|^2 < \epsilon \quad (24)$$

where, $\hat{K}(Z;Z') = \sum_{n=1}^{N} k_n f_n(Z) g_n(Z')$ is the approximate kernel, $\{f_n\}$ and $\{g_n\}$ are two sets of arbitrary orthonormal bases and k_n is the projection of the kernel onto the bases.

However, in practice the number of eigenfunctions is fixed. Then (24) is equivalent to the MMSE problem for a fixed N,

$$\underset{\hat{K}}{\arg\min} \quad \mathbb{E}\{\|K(Z;Z') - \hat{K}(Z;Z')\|^2\} \quad (25)$$

We solve this problem by proving that the approximate kernel, $\hat{K}$ reconstructed from the eigenfunctions obtained using HOGMT is optimal in MMSE sense, which is given in Theorem 1. The choice and trade-offs regarding N are discussed in Section V and evaluated in Section VII.

Theorem 1. *(Eigenfunction approximation for asymmetric kernel) If $K(Z;Z')$ is an asymmetric kernel, approximating it using eigenfunctions decomposed by HOGMT solves (25).*

Proof. Denote $\epsilon_N = \mathbb{E}\{\|K(Z;Z') - \hat{K}(Z;Z')\|^2\}$. Then the total ϵ_N across all DoF is given by,

$$\iint \epsilon_N \, dZ \, dZ'$$

$$= \iint \mathbb{E}\{\left[K(Z;Z') - \sum_{n=1}^{N} k_n f_n(Z) g_n(Z')\right]^2\} \, dZ \, dZ'$$

$$= \iint \mathbb{E}\{\left[K(Z;Z')\right]^2\} \, dZ \, dZ' - \sum_{n=1}^{N} \mathbb{E}\{k_n^2\} \quad (26)$$

As the first term is unrelated to the choice of $\{f_n\}$ and $\{g_n\}$, the problem in (25) is equivalent to maximizing the second term in (26) with the following constraints,

$$\underset{\{f_n\},\{g_n\}}{\arg\max} \quad \sum_{n=1}^{N} \mathbb{E}\{k_n^2\}$$
$$\text{s.t.} \quad \langle f_n, f_{n'} \rangle = \delta_{nn'}, \langle g_n, g_{n'} \rangle = \delta_{nn'} \quad (27)$$

Now, since by definition, k_n is the projection of the kernel onto the bases, we rewrite the objective function in (27) as,

$$\sum_{n=1}^{N} \mathbb{E}\{\left[\iint K(Z;Z') f_n^*(Z) g_n^*(Z') \, dZ \, dZ'\right]^2\} \quad (28)$$

Spatio-temporal eigenfunctions
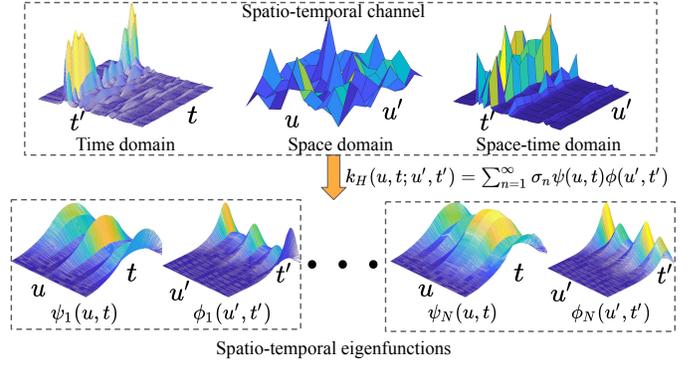
Figure 4: A spatio-temporal 4-D channel is decomposed into two 2-D eigenfunction pairs for Tx and Rx respectively.

Since maximizing a squared term is equivalent to maximizing its absolute value, we introduce a Lagrangian multiplier $\frac{1}{2}\beta_n$ associated with the constraint for f_n and maximize $\mathcal{E}$ as,

$$\mathcal{E} = \sum_{n=1}^{N} \mathbb{E}\{\left| \iint K(Z;Z') f_n^*(Z) g_n^*(Z') \, dZ \, dZ' \right.$$
$$\left. - \frac{1}{2}\beta_n\left(\int f_n(Z) f_n^*(Z) \, dZ - 1\right)\right|\} \quad (29)$$

Differentiating with respect to each f_n^* and setting the derivative to 0 yields,

$$\frac{\partial \mathcal{E}}{\partial f_n^*(Z)} =$$
$$\mathbb{E}\{\left|\int\left(\int K(Z;Z') g_n^*(Z') \, dZ' - \beta_n f_n(Z)\right) dZ\right|\} = 0 \quad (30)$$

which is satisfied when

$$\int K(Z;Z') g_n^*(Z') \, dZ' = \beta_n f_n(Z) \quad (31)$$

(31) proves that the dual eigenfunctions obtained from HOGMT with the property in (23) is indeed a solution to the problem posed in (25) [4]. $\qquad \square$

Figure 4 shows an example of HOGMT approximation for the time-varying MIMO channel, where the time domain shows the time-delay profile, the space domain shows the channel gain between MIMO antennas and the space-time domain shows the delay profile across antennas. Unlike 1-dimensional eigenvectors in the MIMO (spatial) channel matrix, the spatio-temporal Eigenwaves are 2-dimensional, achieving joint orthogonality in space-time domain.

Since the symmetric channel kernel is a special case of the asymmetric channel kernel, Theorem 1 can also approximate symmetric kernels using Mercer's theorem [36].

Corollary 1. *(Special case: symmetric kernel) Specifically, if the kernel $K(Z;Z')$ is symmetric, then decomposing by Mercer's theorem minimizes the kernel approximation error.*

[4] Note that introducing Lagrangian multiplier for g_n and deriving with respect to each g_n^* results in the dual form of (31) which reinforces the duality property of f_n and g_n, leading to the same proof of optimality.

(a) Parallel subchannels in eigen domain   *(b) Practical implementation with HOGMT*
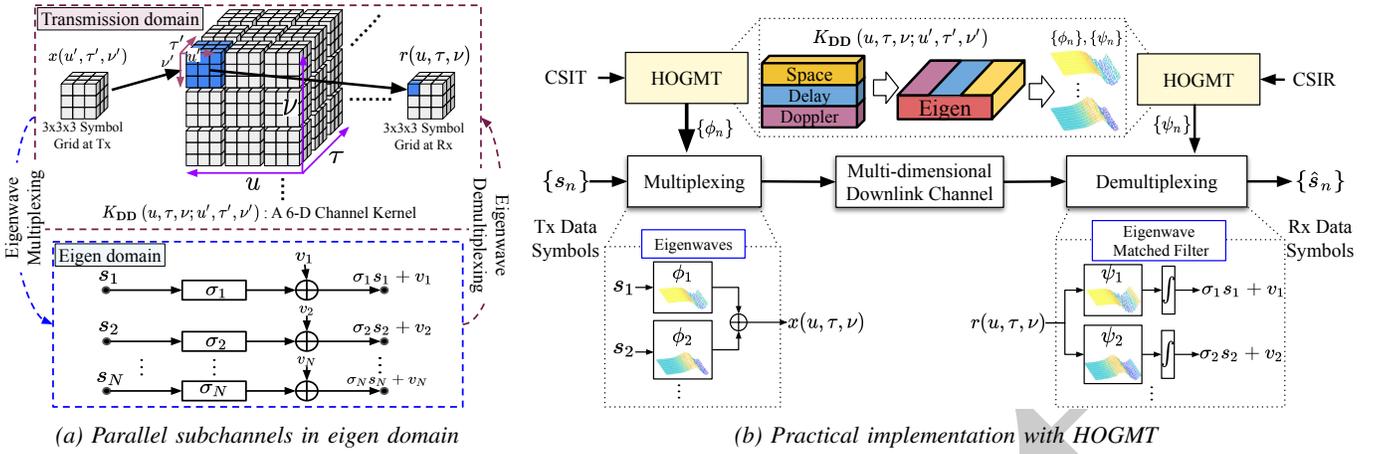
Figure 5: Two views of eigenwave multiplexing: a) Transmission and eigen domain view of a 6-D MIMO-OTFS channel kernel with $u=u'=3, \tau=\tau'=3, \nu=\nu'=3$; b) System view for practical implementation with HOGMT

Proof. For a symmetric kernel, we have the decomposition,

$$\hat{K}(Z;Z')=\sum_{n=1}^{N} k_n f_n(Z)f_n(Z') \tag{32}$$

Following the steps in proof of Theorem 1, we have

$$\int K(Z;Z')f_n^*(Z')\ dZ'=\beta_n f_n(Z) \tag{33}$$

which is the very definition of the eigenfunction f_n, hence suggesting (32) approximated by Mercer's theorem resulting in MMSE of the approximate kernel $\hat{K}$. ∎

Since, Theorem 1 is applicable to all kernels, we always consider asymmetric kernels in our analyses.

V. EIGENWAVE TRANSFORM AND MULTIPLEXING

HOGMT in Section III-C and the subsequent discussions provide a principled approach to combine all the DoF of the channel embodied in its kernel, into one eigen domain. The eigen domain is then divided into independent subchannels, called *Eigenwaves*. Figure 5a shows signal transmission over a 6-D channel kernel. The transmission domain may involve physical processing blocks where signals are convolved over the multi-dimensional channel. Since the DoF at the Tx and Rx are the same, the transmitted symbols, $x(u',\tau',\nu')$ (different from baseband modulated symbols) are arranged in a 3-D grid. This 3-D grid integrates over the 3-D kernel block (blue) across its DoF (u',τ',ν') during convolution and produces a (blue) cube in the received 3-D symbol grid. To obtain each cube across the DoF (u,τ,ν) at the receiver, the 3-D block kernel with DoF (u',τ',ν') should be arranged across DoF (u,τ,ν) leading to a 6-D kernel tensor. Therefore, the kernel is decomposed into parallel Eigenwaves by HOGMT and data-symbols, $\{s_n\}$ are multiplexed over these in the eigen domain. Figure 5b shows an implementation view using HOGMT for decomposing the kernel, obtained from the Channel State Information at the Transmitter (CSIT). This process of multiplexing and demultiplexing and converting the

data symbols between the transmission and the eigen domain is detailed in Section V-B.

From Theorem 1, we learned that HOGMT can also approximate a kernel by a finite number of Eigenwaves (N) ordered by descending eigenvalues. Therefore, transmitting signals over Eigenwaves with N eigenvalues achieve the highest subchannel gains (σ_n). A large value of N will increase the complexity of HOGMT and increase the BER. In contrast, a small N will reduce the throughput. There are multiple strategies for choosing N with respect to different priorities such as memory, complexity, BER or throughput. This trade-off is discussed and evaluated in Section VI-C and Section VII.

A. Eigenwave Transform

OFDM and OTFS utilize FT and SFT to transform the subcarrier domain and the transmission domain, respectively. However, these can not be applied to the eigen domain due to the non-equivalence of Eigenwaves and Fourier bases for LTV channels (this is detailed in Remark 3 in Section V-B). Therefore, to employ Eigenwave as subcarriers, it is necessary to introduce a transform, called Eigenwave Transform to transfer baseband symbols from eigen to transmission domain.

Theorem 2. *Given a continuous signal $x(Z')$ and a discrete eigen space $\mathbb{H}_\Phi$ spanned by Eigenwaves $\phi_n(Z')$, Eigenwave Transform (ET) is defined as the transformation of the transmission domain (Z') to the eigen domain (n) as*

$$x_n=\mathbb{ET}\big[x(Z')\big]=\int x(Z')\phi_n(Z')\ dZ' \tag{34}$$

where x_n is the Eigen form of $x(Z')$ in the eigen space $\mathbb{H}_\Phi$. Then the Inverse Eigenwave Transform (IET) is given by

$$x(Z')=\mathbb{IET}\big[x_n\big]=\sum_{n=1}^{\infty} x_n\phi_n^*(Z') \tag{35}$$

where $\mathbb{ET}[\cdot]$, $\mathbb{IET}[\cdot]$ are the ET, IET operators, respectively[5].

---

[5]The formal expression of ET of $x(Z')$ onto $\phi_n(Z')$ is $\mathbb{ET}_\Phi[x(Z')]$; ET of $r(Z)$ onto $\psi_n(Z)$ is $\mathbb{ET}_\Psi[r(Z)]$. To simplify, we omit the subscript Φ and Ψ, as in this paper, ϕ_n and ψ_n is tied with (Z') and (Z), respectively.

Proof. For ET and IET to be an invertible transform pair, $x_n = \mathbb{ET}\big[\mathbb{IET}\big[x_n\big]\big]$ and $x(Z') = \mathbb{IET}\big[\mathbb{ET}\big[x(Z')\big]\big]$ must hold true. This is detailed in the Appendix A. $\square$

ET is a formal way to derive MEM. As a new proposed operation, its properties are still under investigation. Here, we provide two properties in Corollary 2 and Corollary 3 as complementary support to the multiplexing technique.

Corollary 2. *(Linearity of Eigenwave Transform) ET is a linear operation that satisfies,*

$$\mathbb{ET}\big[ax(Z') + by(Z')\big] = a\mathbb{ET}\big[x(Z')\big] + b\mathbb{ET}\big[y(Z')\big] \quad (36)$$

which also holds for IET as well.

Proof. The proof is provided in the Appendix B. $\square$

Corollary 3. *(Parseval's Theorem in Eigenwave Transform) The integral of the product of two functions (one is the conjugate form) is equal to the sum of its ET transform as*

$$\int x(Z')y^*(Z') \, dZ' = \sum_{n=1}^{\infty} x_n y_n^* \quad (37)$$

Specifically, let $x(Z') = y(Z')$, we have

$$\int |x(Z')|^2 \, dZ' = \sum_{n=1}^{\infty} |x_n|^2 \quad (38)$$

Proof. The proof is provided in the Appendix C. $\square$

Corollary 2 allows for multiplexing parallel Eigenwaves for modulation purposes. Corollary 3 suggests that the energy of signals in the multi-dimensional domain (Z') is equal to the energy of signals in the eigen domain (n).

B. Multi-dimensional Eigenwave Multiplexing

So far, Theorem 1 provides the theoretical support for decomposing finite Eigenwaves and Theorem 2 transfers eigen domain to transmission domain, we formally introduce MEM.

Theorem 3. *(Multi-dimensional Eigenwave Multiplexing) Given a multi-dimensional channel kernel $K(Z;Z')$ with input-output relation as in (20), is decomposed into finite multi-dimensional Eigenwaves in MMSE sense as,*

$$K(Z;Z') = \sum_{n=1}^{N} \sigma_n \psi_n(Z)\phi_n(Z') \quad (39)$$

then, a given symbol set, $\{s_n\}$ is modulated using Eigenwaves $\{\phi_n^*\}$ as subcarriers given by its IET,

$$s(Z') = \mathbb{IET}\big[s_n\big] = \sum_{n}^{N} s_n \phi_n^*(Z') \quad (40)$$

The received signal $r(Z)$ is demodulated by employing the Eigenwave Matched Filter using $\{\psi_n^*\}$ and ET,

$$r_n = \mathbb{ET}\big[r(Z)\big] = \sigma_n s_n + v_n \quad (41)$$

where, v_n is the AWGN noise.

Proof. At the transmitter, the generic symbols $x(Z)$ is obtained by multiplexing the data symbols $\{s_n\}$ and Eigenwaves $\{\phi_n^*(Z)\}$ corresponding to the Z DoF as,

$$x(Z) = \mathbb{IET}\big[s_n\big] = \sum_{n=1}^{N} s_n \phi_n^*(Z) \quad (42)$$

The orthogonality and duality of the eigenfunctions, ensure that the data symbols remain orthogonal from each other after transmission over the multi-dimensional channel, while the corresponding Eigenwaves are transferred to its dual Eigenwaves by the kernel. Considering infinite eigenfunctions for the kernel (ideal case) but a finite number for the transmitted signal (practical case) and no noise (for brevity), the signal at the receiver with Z' DoF is given by the convolution integral (see the Remark 2 in Section III-B),

$$
\begin{aligned}
r(Z) &= \int K(Z;Z')x(Z') \, dZ' \\
&= \int \left\{ \underbrace{\sum_{n=1}^{\infty} \sigma_n \psi_n(Z)\phi_n(Z')}_{\text{decomposed kernel}} \underbrace{\sum_{n'=1}^{N} s_{n'}\phi_{n'}^*(Z')}_{\text{transmitted symbols}} \right\} \, dZ' \\
&= \int \left\{ \sum_{n=1}^{N} \sigma_n s_n \psi_n(Z) \underbrace{|\phi_n(Z')|^2}_{=1} \right. \\
&\quad \left. + \sum_{n=1}^{\infty}\sum_{n' \neq n}^{N} \sigma_n s_{n'} \psi_n(Z) \underbrace{\phi_n(Z')\phi_{n'}^*(Z')}_{=0} \right\} \, dZ' \\
&= \sum_{n=1}^{N} \sigma_n s_n \psi_n(Z) \quad (43)
\end{aligned}
$$

Therefore, (43) shows that the received signal is essentially a projection of the baseband symbols on the eigenspace spanned by the eigenfunctions $\{\phi_n\}$ and the channel transfers it to its dual eigenfunction $\{\psi_n\}$, scaled by gain of parallel subchannel $\{\sigma_n\}$. In this process the data-symbols $\{s_n\}$ are still kept independent in the eigen domain and can be recovered by demultiplexing as shown in Figure 5a.

At the receiver, the received signal $r(Z)$ is projected back to the baseband signal space by multiplying with the conjugate of the dual eigenwave,

$$
\begin{aligned}
r_n &= \mathbb{ET}\big[r(Z)\big] = \int r(Z)\psi_n^*(Z) \, dZ \\
&= \int \sum_{n'=1}^{N} \sigma_{n'} s_{n'} \psi_{n'}(Z)\psi_n^*(Z) \, dZ = \int \sigma_n s_n |\psi_n(Z)|^2 \, dZ \\
&\qquad\qquad\qquad\qquad\qquad\qquad\qquad\qquad = \sigma_n s_n \quad (44)
\end{aligned}
$$

The symbol r_n is an estimate of the original transmitted data symbol, scaled by the channel gain without any interference from other symbols along all the DoF. This is precisely the property of a matched filter but using Eigenwaves of the CSIR decomposed by HOGMT, which is highlighted in Figure 5b as *Eigenwave Matched Filter*. $\square$

Transmitting the modulated symbol $\{s_n\}$ over the multi-dimensional channel with kernel $K(Z;Z')$, the received signal is obtained by (43). Demodulating $r(Z)$ with $\psi_n^*(Z)$, the estimated data r_n is given by (44), which suggests that the demodulated symbol r_n is the data symbol s_n multiplied a scaling factor (channel gain) σ_n along with AWGN, meaning there is no interference from other symbols.

Although, we assume perfect channel estimation and CSIT=CSIR, it is not the focus of this work. Also, the CSIT and CSIR errors are equivalent to the approximation error of $\{\hat{\phi}_n\}$ and $\{\hat{\psi}_n\}$ obtained from HOGMT, which is discussed in Sections VI-A and VII.

Corollary 4. *(Special case: MEM in LTI) In Linear Time-Invariant (LTI) channels, OFDM is a specific case of MEM, where the Eigenwaves do not depend on the specific channel.*

Proof. From the equation (10), we have

$$\mathbf{F}_M \mathbf{h} \mathbf{F}_M^H = \mathbf{b} \implies \mathbf{h}\mathbf{F}_M^H = \mathbf{F}_M^H \mathbf{b} \tag{45}$$

In the LTI channels, the delay taps do not change, meaning $\mathbf{h}$ is a circulant matrix (by adding cycle prefix). Therefore, $\mathbf{b} = \mathbf{F}_M \mathbf{h} \mathbf{F}_M^H$ is a diagonal matrix. Then each column of $\mathbf{F}_M^H$ in (45) is written as

$$\mathbf{h}\mathbf{f}_m = b_m \mathbf{f}_m \tag{46}$$

where b_m is the m-th diagonal element of $\mathbf{b}$. (46) is the definition of eigenvector $\mathbf{f}_m$. Then the IFFT step in OFDM is equivalent to the IET step (40) in MEM. Furthermore, the only requirement to satisfy (46) is that $\mathbf{h}$ is LTI, suggesting that $\mathbf{f}_m$ is the eigenwave for all LTI channels. $\qquad \square$

Remark 3. *From a theoretical stand-point there can be other forms of MEM in LTI channels as the channel can be decomposed into different sets of Eigenwaves. However, the DFT operator ($\mathbf{F}$), employed in OFDM contains the common Eigenwaves of all LTI channels, thus avoiding the need for eigen decomposition. However, for LTV channels, $\mathbf{b}$ in (45) is not diagonal and (46) does not hold. This implies that the complex exponentials are no longer Eigenwaves and the OFDM subcarriers are not orthogonal and hence suffer from ICI. In contrast to OFDM subcarriers being Eigenwaves of LTI channels, OTFS subcarriers are not the common Eigenwaves for the general LTV channels, resulting in IDI.*

Conventional methods define orthogonal subcarriers in a specific domain, which does not ensure interference-free performance unless they satisfy the definition of Eigenwaves of the channel kernel. Therefore, MEM reveals the inner properties of optimal subcarriers for all multi-dimensional channels to achieve orthogonality in the eigen domain and by extension across all DoF. To the best of our knowledge, there is no evidence in the literature showing the existence of common Eigenwaves for LTV channels. *Therefore, for general LTV channels, MEM based on HOGMT decomposition is the only way to obtain and employ Eigenwaves as optimal subcarriers.*

VI. PERFORMANCE ANALYSIS

A. Symbol Error Analysis

The symbol error in MEM is not straight-forward to formulate as it may result from multiple aspects such as CSIT error, CSIR error and approximation error, which motivates us to find a unified metric to characterize all these errors. As the CSI error can also be decomposed into Eigenwaves, it is straightforward that all these errors can be equivalent to the error in the Eigenwaves. Notice that all decomposed Eigenwaves are normalized and thus the error of Eigenwaves is represented by the dependence among Eigenwaves. So, we define the Soft Orthogonality (SO) metric as the measure of the Eigenwave error.

Definition 1. *Soft orthogonality of the normalized basis function $\Phi = \{\phi_n\}_{n=1}^N$ is defined as*

$$O(\Phi) = \frac{1}{N(N-1)} \sum_{n=1}^N \sum_{n' \neq n}^N |\langle \phi_n, \phi_{n'} \rangle| \tag{47}$$

where the best case is $O(\Phi)=0$, meaning the bases are strictly orthogonal and the worst case is $O(\Phi)=1$, indicating all the bases are the same.

Ideally, all the Eigenwaves are strictly orthogonal and joint interference is fully canceled as in (44). However, once there exist CSI errors discussed above, decomposed Eigenwaves would also have errors, denoted as $\{\hat{\phi}_n\}$ and $\{\hat{\psi}_n\}$ so that $O(\hat{\Phi}) \neq 0$ and $O(\hat{\Psi}) \neq 0$. Consequently, using the correlated Eigenwaves for demultiplexing is not perfectly matched with the dual used for multiplexing, leading to symbol error in the transmission domain. So, (44) is rewritten as,

$$\hat{s}_n = \sigma_n s_n + \sum_{n' \neq n}^N \sigma_{n'} s_{n'} R_{\hat{\psi}_{n'}, \hat{\psi}_n^*} \tag{48}$$

where $R_{\hat{\psi}_{n'}, \hat{\psi}_n^*} = \int \hat{\psi}_{n'}(Z) \hat{\psi}_n^*(Z) dZ$ is the correlation of $\hat{\psi}_n$ and $\hat{\psi}_{n'}$. The summation term in (48) serves as a measure of interference from other symbols. Although it may appear that the interference is only expressed by the orthogonality of $\{\hat{\psi}_n\}$, it is also related to that of $\{\hat{\phi}_n\}$. Since the approximate Eigenwaves at the output of HOGMT also possess the *duality* property according to Theorem 1, it is impossible to obtain orthogonal $\{\hat{\psi}_n\}$ from non-orthogonal $\{\hat{\phi}_n\}$ and vice-versa. Therefore, like dual-orthogonality, dual non-orthogonality also impacts multiplexing and demultiplexing in a similar manner.

B. Generality of MEM

Stationary channels: Assuming the channel is ergodic, as it is divided into N independent subchannels (for non-singular channel matrix/tensor, N is the product of the length of each dimension), the capacity of MEM is the sum capacity of N subchannels. Then the average capacity is given by,

$$\bar{C} = \max_{\{P_n\}} \frac{1}{T} \sum_{n=1}^N \log_2 \left(1 + \frac{P_n \lambda_n}{N_0}\right) \tag{49}$$

where, λ_n is n-th eigenvalue and $\mathbb{E}\{\sigma_n\sigma_{n'}\}=\lambda_n\delta_{nn'}$. T is the time length. P_n and N_0 is the power of s_n and v_n, respectively. (49) shows that, with water-filling algorithm, MEM achieves the capacity for stationary channels.

Remark 4. *MEM modulation achieves the sum rate in eigenspace, where Eigenwaves are independent subchannels. It also implies achieving the diversity gain in eigenspace.*

Non-stationary channels: The capacity for non-stationary channels is not well defined as the ergodic assumption does not hold. In this case, we give a qualitative analysis of the optimality by using the concept of *"diversity achieving"* for the non-stationary wireless channels. From [7], we know that the total channel gain for the channel kernel $K(Z;Z')$ is,

$$\iint |K(Z;Z')|^2 \; dZ \; dZ' = \sum_{n=1}^{N} \lambda_n + \epsilon_{MMSE} \qquad (50)$$

where, $\epsilon_{MMSE}=\sum_{n=N+1}^{\infty} \lambda_n$ is the residual channel gain in MMSE sense. The deduction of (50) is given in Appendix D. The power over all demodulated symbol r_n in (43) is,

$$\mathbb{E}\left\{ \left|\sum_{n=1}^{N} r_n\right|^2 \right\} = \sum_{n=1}^{N} \lambda_n P_n + N_0 \qquad (51)$$

From (50) and (51) we find that the data symbol $\{s_n\}$ has leveraged the maximum diversity gain in MMSE.

Higher dimensional channels: The diversity of the multi-dimensional channel at each DoF (space, time-frequency, Doppler-delay, etc.) are merged (integral along each DoF as in (50)) and then divided in the eigenspace into independent Eigenwaves as shown in the dashed block in Figure 5b. Therefore, Eigenwaves achieve diversity in eigenspace, implying that *"diversity achieving"* for the total channel as well.

C. BER and Throughput Trade-off

It is well known that transmitting symbols over subchannels with small subchannel gains results in noise enhancement at the receiver, which is synonymous to Eigenwaves and eigenvalues in MEM. Therefore, choosing proper Eigenwaves as data carriers is desirable to minimize noise enhancement and the BER. We propose a strategy called Zero-padded MEM (ZP-MEM), which assigns *zeros* on Eigenwaves with the smaller eigenvalues, thereby discarding the *bad* subchannels.

Proposition 2. *(ZP-MEM) Given N Eigenwaves ranked in descending order of eigenvalues, ZP-MEM transmits symbols in $\hat{N}<N$ Eigenwaves. The error rate for M-QAM modulated symbol transmitted over the Eigenwave with gain $\sigma_{\hat{N}}$ is[6],*

$$Pr(M, Z', \sigma_{\hat{N}}) \approx 4Q\left(\sigma_{\hat{N}}\sqrt{3Z'/M-1}\right) \qquad (52)$$

where Z' is the SNR. Given the desired error probability bound β, then $\hat{N}$ is chosen as the largest integer satisfy the constraint

[6]The standard approximate error rate for M-QAM modulated symbol is given by [37] as $4Q(\sqrt{3Z'/M-1})$. It is straightforward to derive it for symbols with the subchannel gain $\sigma_{\hat{N}}$ as in (52)

Table III: Parameters of Channel-A and Channel-B

Parameter	Value
Channel model	EVA model
Bandwidth	Bw = 960 KHz
Center frequency	$f_c = 5$ GHz
Speed range	$v \in [100, 150]$ km/h
MEM/OTFS symbol size	Doppler-delay bin: $N_\nu \times N_\tau = 10 \times 64$
Symbols per frame	$L_s = 100$
Time-evolution interval	Ch-A: $N_\nu N_\tau / B_w$; Ch-B: N_τ / B_w

$Pr(M, Z', \sigma_{\hat{N}}) < \beta$, *i.e.*,

$$\sigma_{\hat{N}} > Q^{-1}(\beta/4)/\sqrt{3Z'/(M-1)} \qquad (53)$$

which means the error probability of the symbol that is transmitted over the $\hat{N}$-th eigenwave should be less than β.

ZP-MEM is able to improve the BER by reducing the noise enhancement. However, since it does not utilize all the subchannels, it would reduce the throughput. Therefore, there is a trade-off between the throughput and BER for MEM and ZP-MEM. There may exist other strategies for choosing Eigenwaves, which is not the focus of this paper.

VII. EVALUATION AND RESULTS

A. BER and Throughput

We analyze the accuracy of MEM modulations without supplemental detectors and present comparisons to OTFS with SoTA detectors for two rapidly time-varying channels exhibiting varying degrees of time-evolution interval. We demonstrate the generality of our approach for higher-dimensional channels by directly applying MEM modulation to MU-MIMO channels without any additional precoding. In all the simulations, we assume perfect CSI at the transmitter and receiver.

Rapidly time-varying channels: We simulate the channels in Matlab using the Extended Vehicular A (EVA) model with parameters provided in Table III. We compared MEM with OTFS for two channels: 1) Channel-A, where the time-evolution period is $N_\nu N_\tau / B_w$, which is the duration time of *one* MEM/OTFS symbol, and 2) Channel-B with time-evolution of N_τ / B_w (equals to the duration time of one OFDM symbol with 64 subcarriers). In both cases, we generate the Doppler-delay response per time-evolution interval. For a fair comparison, OTFS is equipped with the Time-Frequency Single Tap (TFST) [30] detector and Zero-Padded Maximal Ratio Combining (ZP-MRC) [38] detector, respectively, which also leverage the perfect CSI at the receiver. Additionally, we also implement a ZP-MEM as in Proposition 2, with $1/8$ and $1/4$ symbol ZP length for both the waveforms.

Figure 6a-6d compare the BER of MEM, ZP-MEM, OTFS with TFST and OTFS with ZP-MRC. In channel A with $1/8$ symbol ZP, MEM has similar BER as OTFS with TFST, but a higher BER than both ZP-MEM and OTFS with ZP-MRC. This is because demodulating data symbols on Eigenwaves with least σ_n enhances the noise as well. On the other hand, the ZP-MRC detector can cancel interference among OTFS symbols
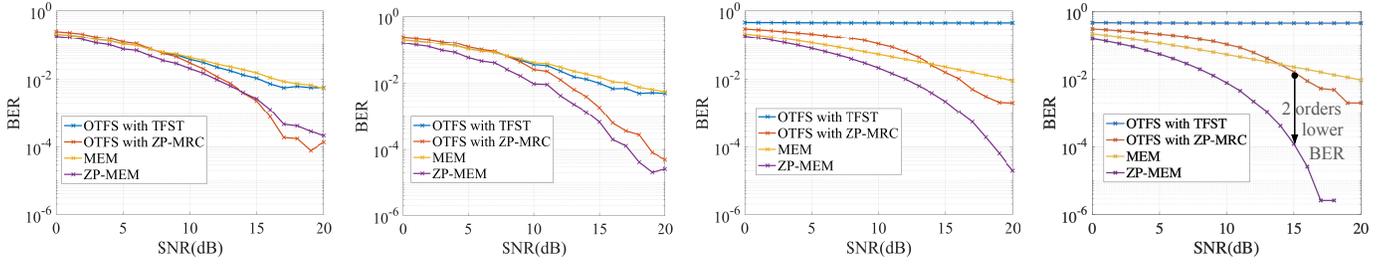
(a) Channel A - 1/8 symbol ZP *(b) Channel A - 1/4 symbol ZP* *(c) Channel B - 1/8 symbol ZP* *(d) Channel B - 1/4 symbol ZP*

Figure 6: BER comparison between MEM and OTFS for Channel-A and Channel-B with QPSK modulation
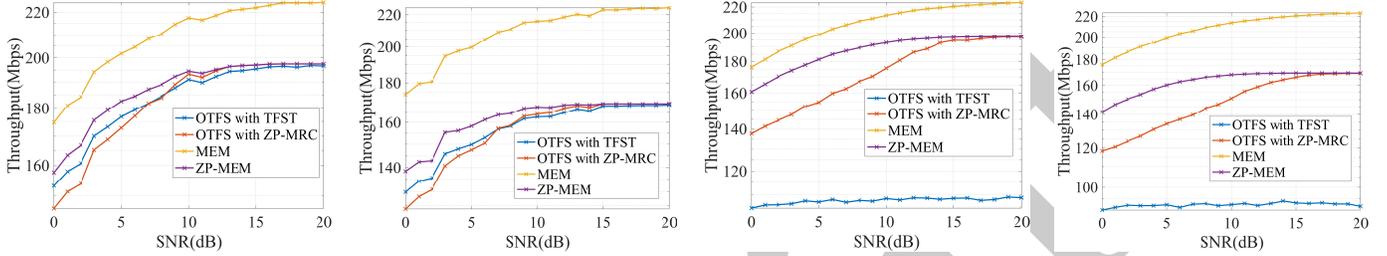
(a) Channel A - 1/8 symbol ZP *(b) Channel A - 1/4 symbol ZP* *(c) Channel B - 1/8 symbol ZP* *(d) Channel B - 1/4 symbol ZP*

Figure 7: Throughput comparison between MEM and OTFS for Channel-A and Channel-B with QPSK modulation

Table IV: Parameters of Channel-C

Parameter	Value
Channel model	3GPP 38.901 UMa NLOS [39]
Array type	BS: 3GPP 3-D [40]; UE: Vehicular [41]
BS antenna	Height $h_b = 10$ m; Number $N_T = 4$
UE antenna	Height $h_u = 1.5$ m; Number $M = 2$
UE number	$K = 2$
UE speed	$v \in [100, 150]$ km/h
Bandwidth	Bw = 20 Mhz
Center frequency	$f_c = 5$ Ghz

(a) BER *(b) Throughput*

Figure 8: Comparing MEM and ZP-MEM in Channel-C

and thus has a similar BER to ZP-MEM. However, as shown in figure 6b, with $1/4$ symbol ZP, ZP-MEM has lower BER due to utilizing better Eigenwaves, minimizing noise enhancement. Figure 6c and 6d show that in the channel B, the TFST detector does not work at all and ZP-MRC detector performs similar to MEM due to more interference in Doppler-delay domain. Both ZP-MEM and MEM are not affected much because interference in the Doppler-delay domain does not affect the orthogonality of Eigenwaves. In this case, ZP-MEM achieves 2 orders of magnitude improvement in BER over OTFS with ZP-MRC at 15dB SNR, which meets the requirement stated in Table I.

Figure 7a-7d show ZP-MEM achieves lower throughput than MEM, since it does not fully utilize all the Eigenwaves. Specifically, with larger ZP, ZP-MEM has a lower throughput, which shows an opposite trend as BER. It provides a trade-off between BER and throughput for MEM and ZP-MEM.

Rapidly time-varying MU-MIMO channel with 6-D kernel (space-Doppler-delay domain): In general, MEM is applicable to any higher-dimensional kernel that may incorporate scattering angles, polarization or any other DoF unique to a particular communication paradigm [34], [35]. The goal of this part is to show its generality without other complementary processing such as precoding. In Channel-C, we choose the space domain

as an additional dimension. As OTFS require precoding to cancel spatial interference, it fails to generalize to higher dimensional channels. Therefore, we do not compare with OTFS in this case. Further, any precoding applied to OTFS can also be applied to MEM, which leads to the same comparison in SISO case in Channel-A and Channel-B. Therefore, we evaluate MEM and ZP-MEM using the 3GPP 38.901 UMa NLOS scenario built on QuaDriga in Matlab. The parameters and the layout of the BE and UE are shown in Table IV.

Figures 8a and 8b show the BER and throughput of MEM and ZP-MEM with QPSK, 16-QAM and 64-QAM modulations. The BER of MEM with QPSK, 16-QAM and 64-QAM are limited to around 10^{-2} as there exist Eigenwaves with significantly low eigenvalues. Note that the power attenuation due to such low subchannel gain cannot be compensated by 10dB increase in SNR resulting in the flat line for MEM with QPSK from 10dB to 20dB SNR. ZP-MEM has lower BER as it does not use those Eigenwaves. However, it achieves lower throughput than MEM. Overall, the performance of MEM and ZP-MEM for Channel-C shows that unlike OTFS, these are applicable to time-varying MU-MIMO channels.

(a) Eigenwaves and One MEM symbol in Doppler-delay domain   (b) One OTFS & MEM symbol   (c) CCDF of PAPR
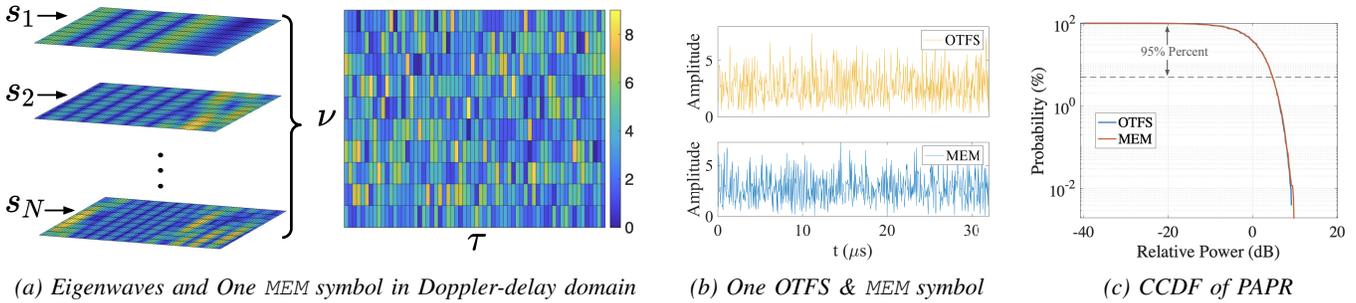
Figure 9: Practicality of MEM: (a) Each MEM symbol is composed of N=64×10 unique Eigenwaves, each multiplied by unique QAM symbols; (b) Time domain OTFS and MEM symbols. In both cases the bandwidth is 20MHz and the Doppler-delay bin size is 10×64, yielding a symbol time of 32μs; (c) PAPR of MEM symbols is statistically similar to OTFS.

B. MEM Symbols in Time Domain

Figure 9a shows an example of MEM Eigenwaves and MEM symbol in the Doppler-delay Domain with a grid size is 10×64. Unlike OFDM and OTFS, the eigenwave is an orthonormal surface across its DoF instead of a unit division in the time-frequency or the Doppler-delay domain. However, from another perspective, consider a Hilbert space, $\mathbb{H}_\Phi$ with basis $\{\phi_n\}$, then each eigenwave can be seen as a unit division in $\mathbb{H}_\Phi$. It means that MEM analyzes the channel as one unified space (eigenspace) instead of multiple subspaces of its DoF. For transmission purposes, the eigenwaves are transferred to the time domain by IFT in the final step. An example time series of one MEM and OTFS symbol are shown in Figure 9b. Both symbols have a bandwidth of 20MHz and a duration of 64/20MHz×10=32μs but use very different subcarriers.

C. Peak to Average Power Ratio (PAPR) of MEM

PAPR is a critical aspect for practical implementation, which is well-investigated in [42]. Figure 9c compares the Complementary Cumulative Distribution Function (CCDF), a metric commonly used to measure PAPR, for both waveforms, any PAPR reduction techniques. The bandwidth is 20MHz and the Doppler-delay bin size is 10×64. It can be seen that both waveforms have very similar PAPR distribution, which is desirable. The dashed line shows the the 95th percentile indicating that the PAPR of MEM is approximately 5 dB.

D. Performance of MEM under Imperfect CSI

We also evaluate the error performance of MEM using a general 4-D channel kernel $K(Z;\Gamma) \in \mathbb{C}^{4\times5\times4\times5}$ with respect to three parameters: Soft Orthogonality, $O(\hat{\Psi})$, SNR and number of Eigenwaves (N). Figures 10a-10e show the change in BER over N. With larger N, the *brighter* region increases because utilizing more Eigenwaves results in higher BER. This is consistent with the observations made in Section VII-A. For each N, the BER increases with $O(\hat{\Psi})$ but decreases with SNR, as Eigenwaves error, measured using the Soft Orthogonality metric, introduces interference from other symbols according to (48). Figures 11a-11e compare the throughput over N. The throughput increases with N, which has an inverse trend of

the BER. The reason is that by using more Eigenwaves, more baseband symbols are multiplexed and transmitted in the same time interval. So, there is a clear trade-off between the BER and the throughput with respect to N. With this flexibility, given a fixed soft orthogonality, we can modify N or improve the SNR to achieve the target performance.

Table V compares the complexity of OFDM, OTFS and MEM in the 2-D case, where N_T and N_F are the number of time and frequency slots, respectively. The number of Eigenwaves $N \leq \min(N_T, N_F)$. The primary computational complexity of MEM arises from the implementation of HOGMT, which is realized by SVD for 2-D channel matrices and by unfolding SVD for 4-D channel tensors.

VIII. CONCLUSION

In this paper, we show the evolution and limitations of current modulation techniques (OFDM, OTFS) for the general LTV channels and propose a novel MEM modulation based on HOGMT decomposition and Eigenwave Transform. This approach employs multi-dimensional Eigenwaves as subcarriers, that are jointly orthogonal across its DoF (*e.g.*, space, time-frequency and Doppler-delay domains). Therefore MEM modulated symbols, when transmitted over multi-dimensional channels do not interfere with each other, without any additional precoding at the transmitter or special detectors at the receiver. We further propose a ZP-MEM method that discards Eigenwaves with lower eigenvalues to reduce the noise enhancement, providing a trade-off between BER and throughput. Evaluation results show that ZP-MEM outperforms OTFS by 2 orders magnitude in BER at 15dB SNR in rapidly time-varying channels. Furthermore, we show the performance of MEM under Eigenwaves error using a novel metric called Soft Orthogonality and under zero error, it achieves the ideal BER and throughput without any interference across all DoF.

Table V: Computational Complexity for modulations

Strategies	Operations	Computational Complexity
OFDM	FFT	$\mathcal{O}(N_T(N_F \log(N_F)))$
OTFS	SFT	$\mathcal{O}((N_T N_F) \log(N_T N_F))$
MEM	ET+HOGMT	$\mathcal{O}(N + \min(N_T N_F^2, N_T^2 N_F))$
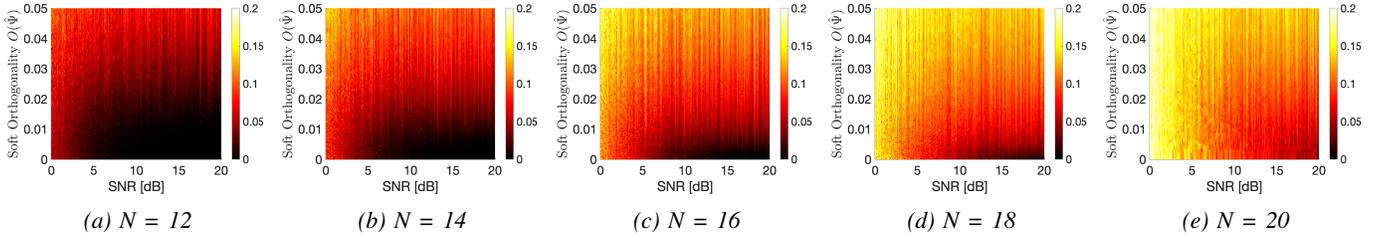
Figure 10: BER of MEM *over SO and SNR for different numbers of Eigenwaves*
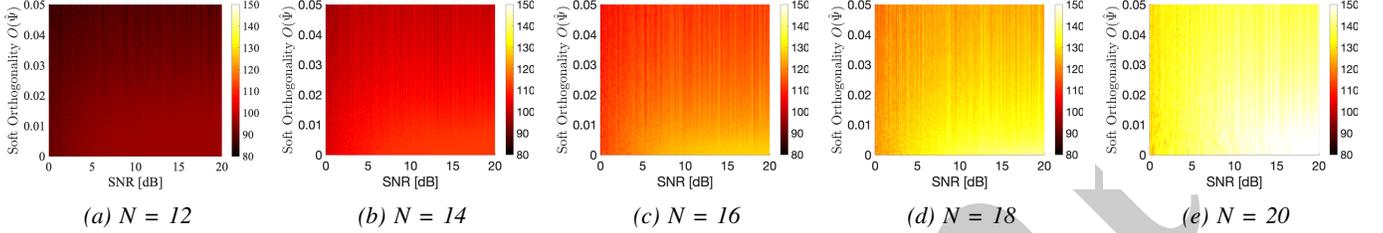
Figure 11: Throughput of MEM *over SO and SNR for different number of Eigenwaves*

APPENDIX A
PROOF OF THEOREM 2

Proof. Given the ET operation $\mathbb{ET}[\cdot]$ defined by (34) and the IET operation $\mathbb{IET}[\cdot]$ defined by (35) with respect to eigenwaves $\phi_n(\Gamma)$, we have

$$\mathbb{ET}\big[\mathbb{IET}[x_n]\big] = \int \sum_{i=1}^{\infty} x_{n'}\phi_{n'}^*(\Gamma)\phi_n(\Gamma) \ d\Gamma$$

$$= \int x_n|\phi_n(\Gamma)|^2 \ d\Gamma + \int \sum_{n'\neq n}^{\infty}\phi_{n'}^*(\Gamma)\phi_n(\Gamma) \ d\Gamma = x_n \quad (54)$$

Meanwhile, we also have

$$\mathbb{IET}\big[\mathbb{ET}[x(\Gamma)]\big] = \sum_{n=1}^{\infty}\left(\int x(\Gamma)\phi_n(\Gamma) \ d\Gamma\right)\phi_n^*(\Gamma)$$

$$= \sum_{n=1}^{\infty}\left(\int \sum_{n'=1}^{\infty}x_{n'}\phi_{n'}^*(\Gamma)\phi_n(\Gamma) \ d\Gamma\right)\phi_n^*(\Gamma)$$

$$= \sum_{n=1}^{\infty}\left(\int x_n|\phi_n(\Gamma)|^2 + \sum_{n'\neq n}^{\infty}x_{n'}\phi_{n'}^*(\Gamma)\phi_n(\Gamma) \ d\Gamma\right)\phi_n^*(\Gamma)$$

$$= \sum_{n}^{\infty}x_n\phi_n^*(\Gamma) = x(\Gamma) \quad (55)$$

Both $x_n = \mathbb{ET}\big[\mathbb{IET}[x_n]\big]$ and $x(\Gamma) = \mathbb{IET}\big[\mathbb{ET}[x(\Gamma)]\big]$ hold, indicating that ET and IET is a transform-pair. $\qquad\square$

APPENDIX B
PROOF OF COROLLARY 2

Proof. By the definition of $\mathbb{ET}[\cdot]$ and $\mathbb{IET}[\cdot]$, we have

$$\mathbb{ET}\big[ax(\Gamma)+by(\Gamma)\big] = \int \big(ax(\Gamma)+by(\Gamma)\big)\phi_n(\Gamma) \ d\Gamma$$

$$= \int ax(\Gamma)\phi_n(\Gamma) \ d\Gamma + \int by(\Gamma)\phi_n(\Gamma) \ d\Gamma$$

$$= a\mathbb{ET}\big[x(\Gamma)\big] + b\mathbb{ET}\big[y(\Gamma)\big] \quad (56)$$

$$\mathbb{IET}\big[ax_n+by_n\big] = \sum_{n=1}^{\infty}\big(ax_n+by_n\big)\phi_n^*(\Gamma)$$

$$= \sum_{n=1}^{\infty}ax_n\phi_n^*(\Gamma) + \sum_{n=1}^{\infty}by_n\phi_n^*(\Gamma) = a\mathbb{IET}\big[x_n\big] + b\mathbb{IET}\big[y_n\big] \quad (57)$$

where (56) and (57) are the very definitions of linearity. $\quad\square$

APPENDIX C
PROOF OF COROLLARY 3

Proof. Applying ET to $x(\Gamma)$ and $y^*(\Gamma)$ in the LHS of (37),

$$\int x(\Gamma)y^*(\Gamma) \ d\Gamma = \int \sum_{n=1}^{\infty}x_n\phi_n^*(\Gamma)\sum_{n'=1}^{\infty}y_{n'}^*\phi_{n'}(\Gamma) \ d\Gamma$$

$$= \int \sum_{n=1}^{\infty}x_ny_n^*|\phi_n(\Gamma)|^2 + \sum_{n}^{\infty}\sum_{n'\neq n}^{\infty}x_ny_{n'}^*\phi_n^*(\Gamma)\phi_{n'}(\Gamma) \ d\Gamma$$

$$= \sum_{n=1}^{\infty}x_ny_n^* \quad (58)$$

which is Parseval's Theorem in Eigenwave Transform. Let $y(\Gamma) = x(\Gamma)$, then (58) is rewritten as, $\int |x(\Gamma)|^2 \ d\Gamma = \sum_{n=1}^{\infty}x_n^2$ $\qquad\square$

APPENDIX D
DEDUCTION OF (50)

$$\iint |K(Z;\Gamma)|^2 \ dZ \ d\Gamma = \iint \left|\sum_{n=1}^{\infty}\sigma_n\phi_n(\Gamma)\psi_n(Z)\right|^2 \ dZ \ d\Gamma$$

$$= \iint \sum_{n}^{\infty}\sigma_n^2\underbrace{|\phi_n(\Gamma)|^2}_{=1}\underbrace{|\psi_n(Z)|^2}_{=1}$$

$$+ \underbrace{\sum_{n'\neq n}^{\infty}\sigma_n\sigma_{n'}\phi_n(\Gamma)\phi_{n'}(\Gamma)^*\psi_n(Z)\psi_{n'}(Z)^*}_{=0} \ dZ \ d\Gamma = \sum_{n=1}^{\infty}\lambda_n$$

12

REFERENCES

[1] Z. Zou, M. Careem, A. Dutta, and N. Thawdar, "Joint Spatio-Temporal Precoding for Practical Non-Stationary Wireless Channels," *IEEE Transactions on Communications*, vol. 71, no. 4, pp. 2396–2409, 2023.

[2] D. Tse and P. Viswanath. Fundamentals of Wireless Communi-cations, 2004.

[3] R. Hadani, S. Rakib, S. Kons, M. Tsatsanis, A. Monk, C. Ibars, J. Delfeld, Y. Hebron, A. J. Goldsmith, A. F. Molisch, and A. R. Calderbank, "Orthogonal time frequency space modulation," *CoRR*, vol. abs/1808.00519, 2018. [Online]. Available: http://arxiv.org/abs/1808.00519

[4] P. Raviteja, K. T. Phan, Y. Hong, and E. Viterbo, "Interference Cancellation and Iterative Detection for Orthogonal Time Frequency Space Modulation," *IEEE Transactions on Wireless Communications*, vol. 17, no. 10, pp. 6501–6515, 2018.

[5] T. Thaj, E. Viterbo, and Y. Hong, "Orthogonal Time Sequency Multiplexing Modulation: Analysis and Low-Complexity Receiver Design," *IEEE Transactions on Wireless Communications*, vol. 20, no. 12, pp. 7842–7855, 2021.

[6] B. C. Pandey, S. K. Mohammed, P. Raviteja, Y. Hong, and E. Viterbo, "Low complexity precoding and detection in multi-user massive MIMO OTFS downlink," *IEEE transactions on vehicular technology*, vol. 70, no. 5, pp. 4389–4405, 2021.

[7] Z. Zou, M. Careem, A. Dutta, and N. Thawdar, "Unified Characterization and Precoding for Non-Stationary Channels," in *ICC 2022 - IEEE International Conference on Communications*, 2022, pp. 5140–5146.

[8] J. Guo, C.-K. Wen, S. Jin, and G. Y. Li, "Overview of Deep Learning-based CSI Feedback in Massive MIMO Systems," 2022. [Online]. Available: https://arxiv.org/abs/2206.14383

[9] Z. Zou and A. Dutta, "Multidimensional Eigenwave Multiplexing Modulation for Non-Stationary Channels," in *IEEE GLOBECOM 2023-IEEE Global Communications Conference*.

[10] G. Matz, "On non-wssus wireless fading channels," *IEEE Transactions on Wireless Communications*, vol. 4, no. 5, pp. 2465–2478, 2005.

[11] F. Hlawatsch and G. Matz, *Wireless Communications Over Rapidly Time-Varying Channels*, 1st ed. USA: Academic Press, Inc., 2011.

[12] J. J. Jaime-Rodríguez, C. A. Gómez-Vega, C. A. Gutiérrez, J. M. Luna-Rivera, D. U. Campos-Delgado, and R. Velázquez, "A non-wssus channel simulator for v2x communication systems," *Electronics*, vol. 9, no. 8, 2020. [Online]. Available: https://www.mdpi.com/2079-9292/9/8/1190

[13] S. Wang, Z. Lu, W. Li, S. Jia, L. Zhang, M. Qiao, X. Pang, N. Idrees, M. Saqlain, X. Gao *et al.*, "26.8-m THz wireless transmission of probabilistic shaping 16-QAM-OFDM signals," *APL photonics*, vol. 5, no. 5, 2020.

[14] M. Kollengode Ramachandran and A. Chockalingam, "MIMO-OTFS in High-Doppler Fading Channels: Signal Detection and Channel Estimation," in *2018 IEEE Global Communications Conference (GLOBECOM)*, 2018, pp. 206–212.

[15] A. RezazadehReyhani, A. Farhang, M. Ji, R. R. Chen, and B. Farhang-Boroujeny, "Analysis of Discrete-Time MIMO OFDM-Based Orthogonal Time Frequency Space Modulation," in *2018 IEEE International Conference on Communications (ICC)*, 2018, pp. 1–6.

[16] S. Srivastava, R. K. Singh, A. K. Jagannatham, and L. Hanzo, "Delay-Doppler and angular domain 4D-sparse CSI estimation in OTFS aided MIMO systems," *IEEE Transactions on Vehicular Technology*, vol. 71, no. 12, pp. 13 447–13 452, 2022.

[17] R. Bomfin, M. Chafii, A. Nimr, and G. Fettweis, "Channel estimation for MIMO space time coded OTFS under doubly selective channels," in *2021 IEEE International Conference on Communications Workshops (ICC Workshops)*. IEEE, 2021, pp. 1–6.

[18] S. Srivastava, R. K. Singh, A. K. Jagannatham, A. Chockalingam, and L. Hanzo, "OTFS transceiver design and sparse doubly-selective CSI estimation in analog and hybrid beamforming aided mmWave MIMO systems," *IEEE Transactions on Wireless Communications*, vol. 21, no. 12, pp. 10 902–10 917, 2022.

[19] D. Shi, W. Wang, L. You, X. Song, Y. Hong, X. Gao, and G. Fettweis, "Deterministic pilot design and channel estimation for downlink massive MIMO-OTFS systems in presence of the fractional Doppler," *IEEE Transactions on Wireless Communications*, vol. 20, no. 11, pp. 7151–7165, 2021.

[20] H. Qu, G. Liu, M. A. Imran, S. Wen, and L. Zhang, "Efficient channel equalization and symbol detection for MIMO OTFS systems," *IEEE Transactions on Wireless Communications*, vol. 21, no. 8, pp. 6672–6686, 2022.

[21] B. Cao, Z. Xiang, and P. Ren, "Low complexity transmitter precoding for MU MIMO-OTFS," *Digital Signal Processing*, vol. 115, p. 103083, 2021.

[22] J. Brown, Jr, "Mean square truncation error in series expansions of random functions," *Journal of the Society for Industrial and Applied Mathematics*, vol. 8, no. 1, pp. 28–32, 1960.

[23] G. W. Stewart, *Matrix Algorithms: Volume II: Eigensystems*. SIAM, 2001.

[24] C. Williams and M. Seeger, "Using the Nyström Method to Speed Up Kernel Machines," in *Advances in Neural Information Processing Systems*, T. Leen, T. Dietterich, and V. Tresp, Eds., vol. 13. MIT Press, 2000. [Online]. Available: https://proceedings.neurips.cc/paper_files/paper/2000/file/19de10adbaa1b2ee13f77f679fa1483a-Paper.pdf

[25] T. Peken, S. Adiga, R. Tandon, and T. Bose, "Deep learning for SVD and hybrid beamforming," *IEEE Transactions on Wireless Communications*, vol. 19, no. 10, pp. 6621–6642, 2020.

[26] Z. Deng, J. Shi, and J. Zhu, "Neuralef: Deconstructing kernels by deep neural networks," in *International Conference on Machine Learning*. PMLR, 2022, pp. 4976–4992.

[27] Z. Zou, I. Amarasekara, and A. Dutta, "Learning to Decompose Asymmetric Channel Kernels for Generalized Eigenwave Multiplexing," in *IEEE INFOCOM 2024-IEEE Conference on Computer Communications*.

[28] P. Almers, E. Bonek, A. Burr, N. Czink, M. Debbah, V. Degli-esposti, H. Hofstetter, P. Kyosti, D. Laurenson, G. Matz, A. F. Molisch, C. Oestges, and H. Ozcelik, *Survey of channel and radio propagation models for wireless MIMO systems*. EURASIP Journal on Wireless Communications and Net-working, 2007.

[29] P. Bello, "Characterization of Randomly Time-Variant Linear Channels," *IEEE Transactions on Communications Systems*, vol. 11, no. 4, pp. 360–393, 1963.

[30] Y. Hong, T. Thaj, and E. Viterbo, *Delay-Doppler Communications: Principles and Applications*, 1st ed. USA: Elsevier Science., 2022.

[31] Y. Li, J. Winters, and N. Sollenberger, "Mimo-ofdm for wireless communications: signal detection with enhanced channel estimation," *IEEE Transactions on Communications*, vol. 50, no. 9, pp. 1471–1477, 2002.

[32] Y. S. Cho, J. Kim, W. Y. Yang, and C. G. Kang, *MIMO-OFDM wireless communications with MATLAB*. John Wiley & Sons, 2010.

[33] S. K. Mohammed, "Derivation of OTFS Modulation From First Principles," *IEEE Transactions on Vehicular Technology*, vol. 70, no. 8, pp. 7619–7636, 2021.

[34] C. Guo, F. Liu, S. Chen, C. Feng, and Z. Zeng, "Advances on Exploiting Polarization in Wireless Communications: Channels, Technologies, and Applications," *IEEE Communications Surveys & Tutorials*, vol. 19, no. 1, pp. 125–166, 2017.

[35] A. Ali, E. De Carvalho, and R. W. Heath, "Linear receivers in non-stationary massive MIMO channels with visibility regions," *IEEE Wireless Communications Letters*, vol. 8, no. 3, pp. 885–888, 2019.

[36] J. Mercer, "Functions of Positive and Negative Type, and their Connection with the Theory of Integral Equations," *Philosophical Transactions of the Royal Society of London. Series A, Containing Papers of a Mathematical or Physical Character*, vol. 209, pp. 415–446, 1909. [Online]. Available: http://www.jstor.org/stable/91043

[37] M. K. Simon and M.-S. Alouini, *Digital communication over fading channels*. New York: Wiley, 2001.

[38] T. Thaj and E. Viterbo, "Low complexity iterative rake decision feedback equalizer for zero-padded OTFS systems," *IEEE transactions on vehicular technology*, vol. 69, no. 12, pp. 15 606–15 622, 2020.

[39] 3GPP TR 38.901 v16.1.0, "5G; Study on channel model for frequencies from 0.5 to 100 GHz," 3rd Generation Partnership Project (3GPP), Tech. Rep., 11 2020.

[40] 3GPP TR 37.885 v15.1.0, "Technical specification group radio access network; study on evaluation methodology of new vehicle-to-everything v2x use cases for lte and nr," 3rd Generation Partnership Project (3GPP), Tech. Rep., 09.

[41] 3GPP TR 36.873 v12.5.0, "Technical specification group radio access network; study on 3d channel model for lte," 3rd Generation Partnership Project (3GPP), Tech. Rep., 06.

[42] S. H. Han and J. H. Lee, "An overview of peak-to-average power ratio reduction techniques for multicarrier transmission," *IEEE Wireless Communications*, vol. 12, no. 2, pp. 56–65, 2005.